Journal of Zhejiang University-SCIENCE A (Applied Physics & Engineering)
ISSN 1673-565X (Print); ISSN 1862-1775 (Online)
www.zju.edu.cn/jzus; www.springerlink.com
E-mail: jzus@zju.edu.cn

Unsteady simulation for a high-speed train entering a tunnel*

Xin-hua LI[1], Jian DENG[†‡2], Da-wei CHEN[2], Fang-fang XIE[1], Yao ZHENG[1]

([1]*School of Aeronautics and Astronautics, Zhejiang University, Hangzhou 310027, China*)

([2]*National Engineering Laboratory for System Integration of High-Speed Train (South), CSR Qingdao Sifang Co., Ltd., Qingdao 266111, China*)

[†]E-mail: zjudengjian@zju.edu.cn

Received Sept. 23, 2011; Revision accepted Sept. 25, 2011; Crosschecked Sept. 26, 2011

Abstract: In order to study the unsteady aerodynamics effects in railway tunnels, the 3D Reynolds average Navier-Stokes equations of a viscous compressible fluid are solved, and the two-equation k-ε model is used in the simulation of turbulence, while the dynamic grid technique is employed for moving bodies. We focus on obtaining the changing tendencies of the aerodynamic force of the train and the aerodynamic pressures on the tunnel wall and train surface, and discovering the relationship between the velocity of the train and the intensity of the micro pressure wave at the tunnel exit. It is shown that the amplitudes of the pressure changes in the tunnel and on the train surface are both approximately proportional to the square of the train speed, so are the microwave and the drag of the train.

Key words: High-speed train, Aerodynamics, Railway tunnel, Numerical analysis
doi:10.1631/jzus.A11GT008 **Document code:** A **CLC number:** U270.1+1; V211

1 Introduction

When a train enters or leaves a tunnel, finite amplitude pressure waves are generated and propagate in the tunnel. At the tunnel exit, the waves are partially reflected. The reflected waves of opposite pressure return into the tunnel and are partly emitted outside the tunnel as a microwave. The air pressure change in and around the tunnel has a great impact on the safe operation of trains, staff comfort, and environment around the tunnel (Joseph, 2001; Tian, 2007). A 1D numerical simulation method was first used to study the pressure variations on the train and in the tunnel (Woods and Pope, 1979; Mei *et al*., 1995; William-Louis and Tournier, 2005). In the 20th century, a series of experiments concerning the pressure changes, microwave, and aerodynamic drag was carried out on the Japanese Shinkansen. In recent years, Japanese researchers have simulated the changes of the pressure and microwave using 3D models and model experiments (Ogawa and Fujii, 1997; Tanaka *et al.*, 2003; Sato and Sassa, 2005; Iida *et al.*, 2006). In Europe, model experiments were performed on the compression wave generated by a train entering a tunnel with different configurations (flared portals, vented portals, vented hoods, etc.) (Ricco *et al.*, 2007; Anthoine, 2009). In China, 3D numerical simulation and model experiments have been used, and the influences of running speed, blocking ratio, train head shape, and railroad condition on the aerodynamic effects have been analyzed (Luo *et al.*, 2004; Zhao *et al.*, 2006; Zhao and Li, 2009; Li *et al.*, 2010; Liu *et al.*, 2010a; 2010b). To date, studies have mainly focused on a speed of 250 km/h and few have examined the aerodynamic effects above 300 km/h. Moreover, 3D effects are rarely taken into account.

In this paper, we solve the 3D Reynolds average Navier-Stokes equations of a viscous compressible fluid, and the dynamic grid technique is employed for moving bodies. The unsteady aerodynamic effects of a high-speed train entering a tunnel are studied to obtain the changes of the pressure and the aerodynamic force. In order to find the relationship between

‡ Corresponding author

* Project (No. 2009BAG12A01) supported by the National Key Technology R&D Program of China

the train speed, and the pressure changes and microwave, we calculate the models at different speeds of 200, 250, 300, 350, 400, 450, and 500 km/h.

2 Fundamental flow equations

When a train passes through a tunnel, the flow field around the train is compressible, viscous, unsteady turbulent flow. For more details of the turbulent flow equations, please refer to (Ferzieger and Peric, 1996). The Reynolds average Navier-Stokes equations are presented as below.

Continuity equation:

$$\frac{\partial \rho}{\partial t}+\frac{\partial(\rho u_j)}{\partial x_j}=0, \quad j=1, 2, 3, \tag{1}$$

where t is the time, ρ is the density, x_j is the cartesian coordinate, and u_j is the absolute fluid velocity component in direction x_j.

Momentum equation:

$$\frac{\partial(\rho u_i)}{\partial t}+\frac{\partial(\rho u_i u_j)}{\partial x_j}=\rho f_i-\frac{\partial p}{\partial x_i}+\frac{\partial \tau_{ij}}{\partial x_j}, \tag{2}$$

where p is the static pressure, u_i is the velocity component in direction x_i, f_i is the mass force component in direction x_i, and τ_{ij} is the stress tensor with the specific expression as

$$\tau_{ij}=\mu\left[\left(\frac{\partial u_j}{\partial x_i}+\frac{\partial u_i}{\partial x_j}\right)-\frac{2}{3}\frac{\partial u_k}{\partial x_k}\delta_{ij}\right], \tag{3}$$

where μ is the viscosity coefficient of the air and δ_{ij} is a unit tensor.

Turbulent kinetic energy (k) equation:

$$\frac{\partial(\rho k)}{\partial t}+\frac{\partial(\rho k u_i)}{\partial x_i}=\frac{\partial\left[\left(\mu+\frac{\mu_t}{\sigma_k}\right)\frac{\partial k}{\partial x_j}\right]}{\partial x_j}+G_k-\rho\varepsilon+G_b-Y_M+S_k. \tag{4}$$

Turbulent dissipation rate (ε) equation:

$$\frac{\partial(\rho\varepsilon)}{\partial t}+\frac{\partial(\rho\varepsilon u_i)}{\partial x_i}=\frac{\partial\left[\left(\mu+\frac{\mu_t}{\sigma_\varepsilon}\right)\frac{\partial \varepsilon}{\partial x_j}\right]}{\partial x_j}+C_{\varepsilon 1}\frac{\varepsilon}{k}(G_k+C_{\varepsilon 3}G_b)-C_{\varepsilon 2}\rho\frac{\varepsilon^2}{k}+S_\varepsilon. \tag{5}$$

3 Computational domain and mesh generation

A simplified geometric model of electric multiple units (EMU) is used in the numerical simulation (Fig. 1). This model removes the bogies, pantograph, and other details of the train. The front shape of the model and the real train match well. The total length of the train model is 76.5 m.

Fig. 2 shows the grids used in the numerical simulation of the train entering a tunnel. The grids are divided into two parts: one part is the moving mesh, which contains the semi-cylindrical region around the train; the other part is the fixed part, which includes the area around the tunnel wall. The sliding interface technology is used to solve the relative motion between the train and the tunnel. The moving mesh moves at the speed of the train. On the direction of the motion, the front boundary deletes grids, while the opposite one adds grids layer-by-layer to make the grids move. The grids have about 1.2 million grid hexahedral elements.

Fig. 1 Simplified geometric model of electric multiple units (EMU)

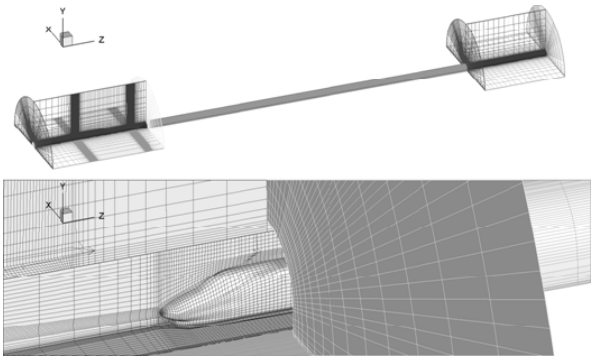

Fig. 2 Grids of a train entering a tunnel

In order to simulate the impact of the turbulent boundary layer, the standard turbulent wall function is adopted. Therefore, the first layer near the wall should meet the requirement of $30<y+<300$ ($y+$ is the non-dimensional parameter of wall) to include it in the logarithmic area of the turbulent boundary layer. According to the velocity and size of the train, the height of the first layer near the wall should be 0.005 m.

4 Results

4.1 Description of the wave propagation process

Fig. 3 shows 25 monitor points that are set on the train. The maximum pressure differences of the monitor points 1–11 and 15–25 are also shown in this figure. The differences of the pressure amplitude between different monitor points are small, and the maximum value of the differences is 147 Pa. Due to the train passing through a double-track tunnel, the distribution of the pressure differences is asymmetrical, and the pressure differences on the side that is closer to the tunnel wall are higher than that of the other side. About the longitudinal distribution of the train, the two sides of the train take on an entirely different distribution. For the side closer to the tunnel wall, the pressure difference amplitude on the middle of the train is smaller than that on the two ends. However, on the other side of the train, the pressure difference amplitude on the middle of the train is higher than that on the two ends.

Fig. 4 shows the pressure change in the tunnel wall and on the train surface when the EMU passes through a tunnel at the speed of 200 km/h. Fig. 4a shows the Mach wave propagation diagram and Fig. 4b shows the pressure history of the measured point 6 on the train surface. This point is presented by the dash-and-dot line in Fig. 4a. Now we focus on the pressure changes on the train surface: point *A* indicates that the initial expansion wave of the train tail reached the point 6; point *B* denotes that the first reflection expansion wave of the train head reached the point 6; point *C* presents that the first reflection compression wave of the train tail reached the point 6; point *D* shows that the second reflection compression wave of the train head reached the point 6; point *E* indicates that the second reflection expansion wave of the train tail reached the point 6; and, points *F*–*J* can

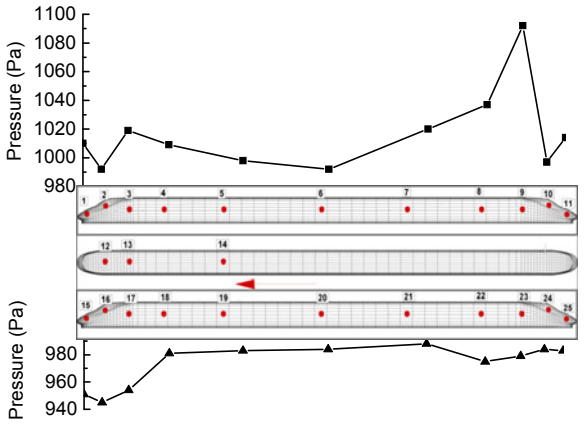

Fig. 3 Twenty five monitor points set on the train surface and the pressure amplitude with the location of the monitor points

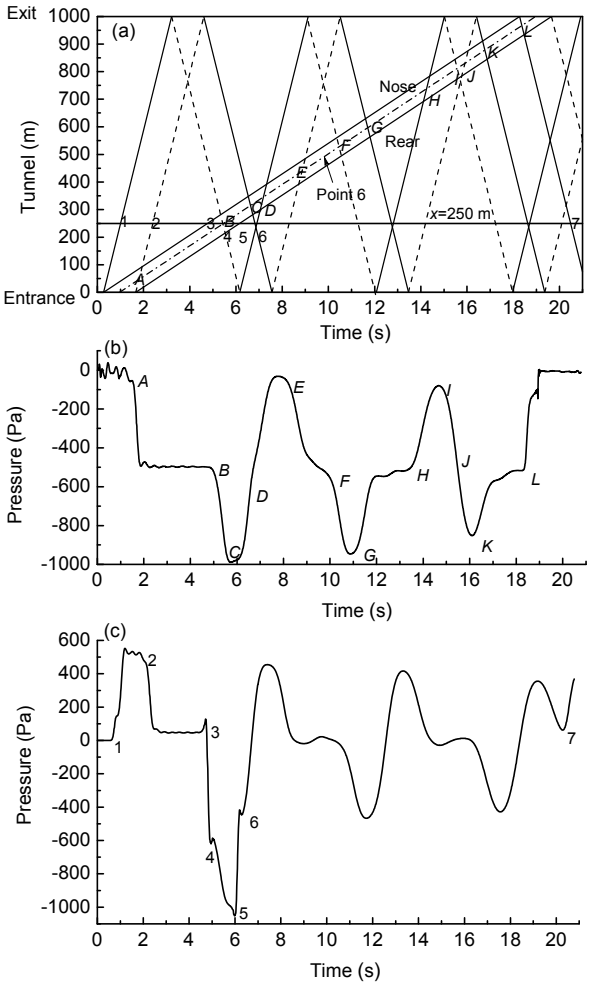

Fig. 4 Wave diagram and pressure transients due to EMU passing through a tunnel at the speed of 200 km/h
(a) Wave diagram; (b) Pressure changes at point 6 on the train; (c) Pressure changes at 250 m in the tunnel

be handled in the same manner. Point *L* indicates that the compression wave of the train head leaving the tunnel reached the point 6. When a compression wave passes through the measuring point, the pressure of the point increases; and when an expansion wave passes through the point, the pressure of the point decreases. We can infer that when the time reaches points *A*, *B*, *E*, *F*, *I*, and *J* in Fig. 4b, the pressure at these points decreases, and when the time reaches points *C*, *D*, *G*, *H*, *K*, and *L* in Fig. 4b, the pressure at these points increases.

Fig. 4c shows the pressure history of the measured point at 250 m from the tunnel entrance, and it is represented by the x=250 m line in Fig. 4a. Point 1 indicates that the initial compression wave of the train head goes through the measured point, the pressure of the measured point increases; point 2 indicates that the initial expansion wave of the train tail goes through the measured point, the pressure of the measured point decreases; point 3 shows that the train head goes through the measured point, the pressure of the measured point decreases; point 4 indicates that the first reflection expansion wave of the train head goes through the measured point, the pressure of the measured point decreases; point 5 reveals that the train tail goes through the measured point, the pressure of the measured point increases; point 6 indicates that the second reflection compression wave of the train head and the first reflection compression wave of the train tail go through the measured point, while the pressure of the measured point increases; and, point 7 denotes that the compression wave of the train head leaving the tunnel goes through the measured point, the pressure of the measured point decreases.

4.2 Pressure difference amplitudes on the train surface and the tunnel wall

Table 1 shows the results of the pressure difference amplitudes on the train surface and the tunnel wall of the train passing through the tunnel at different speeds. The fitting formulas between the pressure difference amplitude (y) and the train speed (x) for these two cases are, respectively, $y=0.017x^{2.08}$ and $y=0.013x^{2.15}$, which indicate that, when the train operates at a higher speed, greater than 200 km/h, the amplitudes of the pressure change on the tunnel wall and the surface of the train are approximately proportional to the square of the train speed.

Table 1 Pressure difference amplitudes on the train surface and tunnel wall

Train speed (km/h)	Pressure difference amplitude (Pa)	
	Train surface	Tunnel wall
200	1027	1169.8
250	1613	1874.5
300	2335	2840.7
350	3199	3716.8
400	4202	4937.6
450	5380	6377.5
500	6751	8264.0
Fitting formula	$y=0.017x^{2.08}$	$y=0.013x^{2.15}$

Fig. 5 compares the numerical simulation results with the on-site test results of pressure change magnitude on the train surface with the train speed. The numerical simulation results approximately conform to the on-site test results. However, the numerical result is still a little higher than the on-site test results.

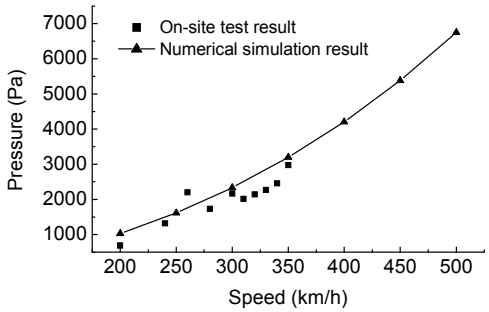

Fig. 5 Pressure difference amplitude on the train surface

4.3 Microwave

The microwave is radiated from the portal toward the outside. Therefore, it is connected with the pressure amplitude of the tunnel exit. Fig. 6a shows the pressure changes at 970 m in the tunnel, which is 30 m away from the tunnel exit. The pressure at this point is taken to stand for the pressure of the tunnel exit. In Fig. 6a, the first wave crest is produced by the initial compression wave of the train head and the first reflection expansion wave of the train head, and the first wave trough is produced by the initial expansion wave of the train tail and the first reflection compression wave of the train tail. The first peak of the microwave is from the first wave crest of the pressure, and the first trough of microwave is from the first wave trough of the pressure.

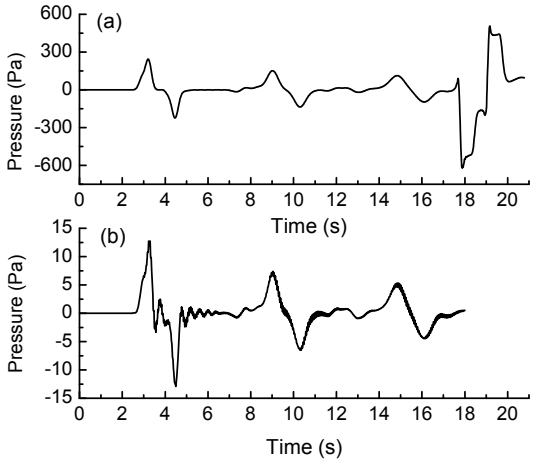

Fig. 6 Pressure changes at 970 m in the tunnel and the microwave history of the tunnel

The amplitude of the first pressure wave of the tunnel exit and the amplitude of the first microwave are compiled as shown in Fig. 7. The fitting lines of the microwave, and changes with the pressure of the tunnel exit, are also presented in Fig. 7. The fitting lines between the microwave amplitude and the amplitude of the pressure are y=−4.6+0.059x (L=15 m, where L is the distance between the test point and the tunnel exit) and y=−5.6+0.046x (L=20 m), respectively. The microwave is approximately proportional to the pressure of the tunnel exit.

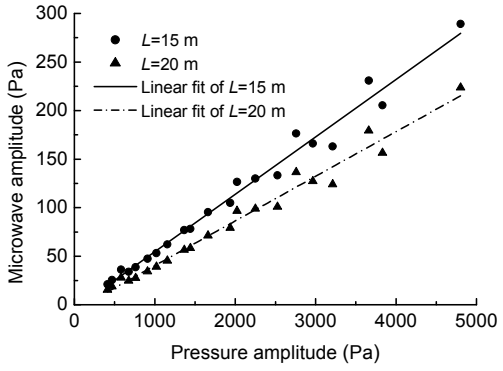

Fig. 7 Microwave change amplitudes with the initial magnitude of tunnel exit pressure

The relationships between the microwave and train speed are shown in Fig. 8. The figure shows that the microwave is approximately proportional to the square of train speed. The fitting formulae between the microwave amplitude and the train speed are y=$1.5\times10^{-4}x^{2.28}$ (L=15 m) and y=$7.9\times10^{-4}x^{2.34}$ (L=20 m), respectively.

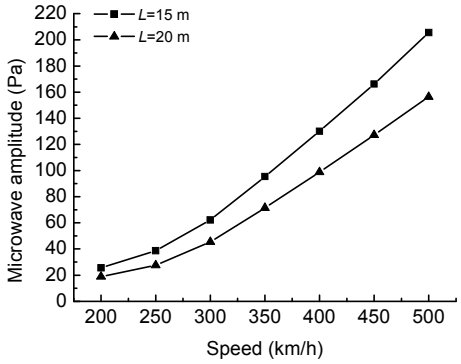

Fig. 8 Microwave change amplitude with the train speed

4.4 Aerodynamic forces of the train

Due to the pressure wave propagation and airflow in the tunnel, the aerodynamic forces are different between the train passing through the double-track tunnel and running on the open line. Fig. 9 shows the results of aerodynamic forces change of the train passing through the tunnel. It can be concluded that the lift force of the train exhibits no significant difference between the cases running on the open line and in the tunnel. The lateral force of the train increases when the train enters the tunnel, and then remains constant after the train entering. When the train leaves the tunnel, the lateral force increases rapidly, and then decreases rapidly to a steady state. The aerodynamic drag increases rapidly when the train enters the tunnel, then fluctuates about a certain value. Compared with the changes of the lateral force and the lift force of the train, the changes of the drag of the train act a complex manner. A detailed analysis on the change of the drag for the train passing through the tunnel is as follows.

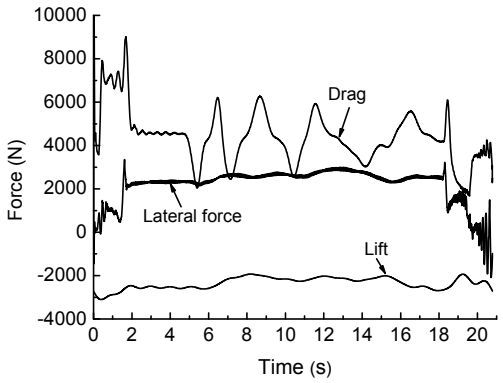

Fig. 9 Aerodynamic forces of the train passing through the tunnel

In Fig. 10, point *A* stands for the train head beginning to enter the tunnel. The pressure of the train head increases, and the drag of the train increases rapidly; point *B* stands for the train tail entering the tunnel. When the whole train enters the tunnel, the pressure of the train tail increases, and the drag of the train decreases; at point *C*, the initial expansion wave of the tail reaches the train head, the pressure of the train head decreases, and the drag of the train decreases; point *D* stands for the first reflection expansion wave of the train head meeting the train head, when the pressure of the train head decreases, and the drag of the train decreases; point *E* stands for the first reflection expansion wave of the train head reaching the train tail, when the pressure of the train tail decreases, and the drag of the train increases; point *F* stands for the train head running out the tunnel, when the pressure of the train head decreases, and the drag of the train decreases; point *G* stands for the compression wave of the train leaving the tunnel meeting the train tail, when the pressure of the train tail increases, and the drag of the train decreases; and, point *H* stands for the whole train leaving the tunnel, when the pressure of the train tail decreases, the drag of the train increases. The expansion wave reaches the train head, the pressure of the train head decreases, and the drag of the train decreases. The compression wave reaches the train head, the pressure of the train head increases, and the drag of the train increases. The expansion wave reaches the train tail, the pressure of the train tail decreases, and the drag of the train increases. The compression wave reaches the train tail, the pressure of the train tail increases, and the drag of the train decreases.

Most researchers analyze the drag of the train varying with the speed of the train. The maximum value of the drag is used, and the amplitude of the drag force is neglected. In this study, we combine the amplitude of the drag and the average value of the drag to analysis the drag variation with train speed. The drag of the train can be represented by Drag= DA±(DB/2), where DA is the average value of the drag, and DB is the amplitude of the drag. Fig. 11 shows the average value of the drag and the amplitude of the drag change with the speed of the train. The fitting formulas between the drag and train speed are y=0.025$x^{2.3}$ and y=0.065$x^{2.1}$, respectively, which show that the average value of the drag and the amplitude of the drag are all approximately proportional to the square of train speed.

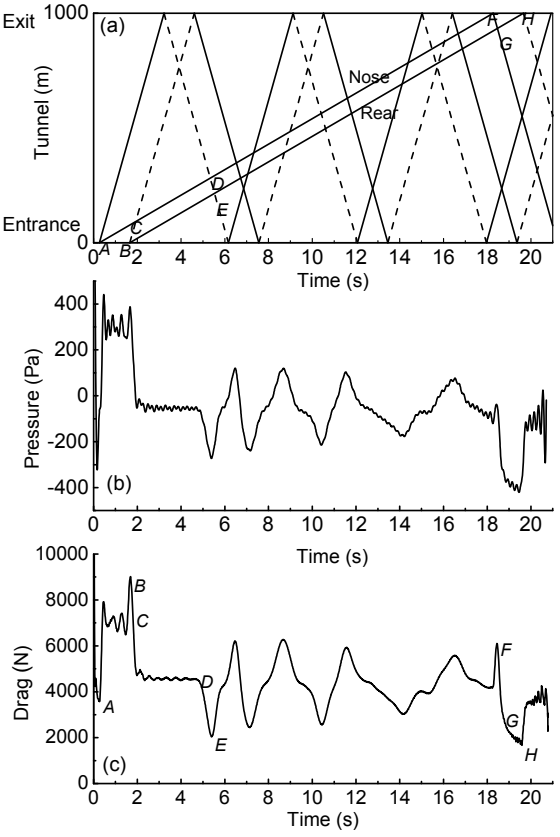

Fig. 10 Wave diagram and drag changes due to EMU passing through a tunnel at the speed of 200 km/h
(a) Wave diagram; (b) Pressure difference between the monitor points 1 and 11; (c) Drag history of the train

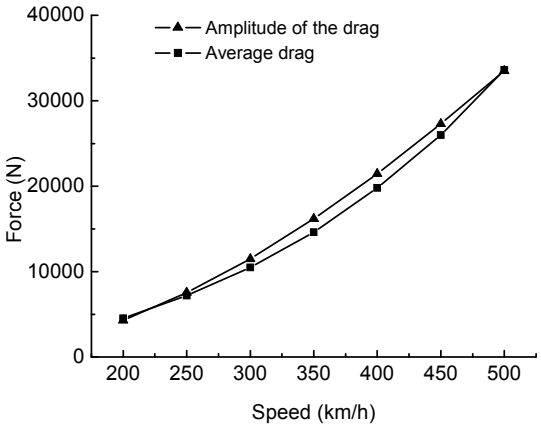

Fig. 11 Drag change with the train speed

5 Conclusions

Via numerical simulation of the train passing through a tunnel, the following conclusions are made:

1. The amplitude of the pressure change on the tunnel wall and in the train surface is approximately proportional to the square of the train speed.

2. The microwave is approximately proportional to the square of train speed.

3. The drag of the train is represented by Drag= DA±(DB/2), where DA is the average value of the drag, and DB is the amplitude of the drag. Both the average value of the drag and the amplitude of the drag are approximately proportional to the square of train speed.

Acknowledgements

The authors are grateful for the assistance in all the numerical computations by the Center for Engineering and Scientific Computation (CESC), Zhejiang University, China.

References

Anthoine, J., 2009. Alleviation of pressure rise from a high-speed train entering a tunnel. *AIAA Journal*, **47**(9): 2132-2142. [doi:10.2514/1.41109]

Ferzieger, J.L., Peric, M., 1996. Computational Methods for Fluid Dynamics. Springer-Verlag, Heidelberg, p.265-328.

Iida, M., Kikuchi, K., Fukuda, T., 2006. Analysis and experiment of compression wave generated by train entering tunnel entrance hood. *JSME International Journal Series B*, **49**(3):761-770. [doi:10.1299/jsmeb.49.761]

Joseph, A.S., 2001. Aerodynamics of high-speed trains. *Annual Review of Fluid Mechanics*, **33**(3):371-414.

Li, R.X., Zhao, J., Liu, J., Zhang, W.H., 2010. Influence of air pressure pulse on side windows of high-speed trains passing each other. *Chinese Journal of Mechanical Engineering*, **46**(4):87-98 (in Chinese). [doi:10.3901/JME.2010.04.087]

Liu, T.H., Tian, H.Q., Liang, X.F., 2010a. Aerodynamic effects caused by trains entering tunnels. *Journal of Transportation Engineering*, **136**(9):846-853. [doi:10.1061/(ASCE)TE.1943-5436.0000146]

Liu, T.H., Tian, H.Q., Liang, X.F., 2010b. Design and optimization of tunnel hoods. *Tunnelling and Underground Space Technology*, **25**(3):212-219. [doi:10.1016/j.tust.2009.12.001]

Luo, J.J., Gao, B., Wang, Y.X., Zhao, W.C., 2004. Numerical simulation of unsteady three dimensional flow induced by high-speed train entering tunnel with shaft. *Journal of Southwest Jiaotong University*, **39**(4):442-446 (in Chinese).

Mei, Y.G., Zhao, H.H., Liu, Y.Q., 1995. Numerical analysis about pressure wave of high-speed train. *Journal of Southwest Jiaotong University*, **30**(6):667-672 (in Chinese).

Ogawa, T., Fujii, K., 1997. Numerical investigation of three-dimensional compressible flows induced by a train moving into a tunnel. *Computers & Fluids*, **26**(6):565-585. [doi:10.1016/S0045-7930(97)00008-X]

Ricco, P., Baron, A., Molteni, P., 2007. Nature of pressure waves induced by a high-speed train travelling through a tunnel. *Journal of Wind Engineering and Industrial Aerodynamics*, **95**(8):781-808. [doi:10.1016/j.jweia.2007.01.008]

Sato, T., Sassa, T., 2005. Prediction of the compression pressure wave generated by a high-speed train entering a tunnel. *International Journal of Computational Fluid Dynamics*, **19**(1):53-59. [doi:10.1080/10618566412331286328]

Tanaka, Y., Iida, M., Kikuchi, K., 2003. Method to simulate generation of compression wave inside a tunnel at train entry with a simple geometry model. *Transactions of the Japan Society of Mechanical Engineers Series B*, **69**(683): 1607-1614 (in Japanese). [doi:10.1299/kikaib.69.1607]

Tian, H.Q., 2007. Train Aerodynamics. China Railway Publishing House, Beijing, China, p.268-303 (in Chinese).

William-Louis, M., Tournier, C., 2005. A wave signature based method for the prediction of pressure transients in railway tunnels. *Journal of Wind Engineering and Industrial Aerodynamics*, **93**(6):521-531. [doi:10.1016/j.jweia.2005.05.007]

Woods, W.A., Pope, C.W., 1979. On the Range of Validity of Simplified One Dimensional Theories for Calculating Unsteady Flows in Railway Tunnels. The 3rd International Symposium on the Aerodynamics and Ventilation of Vehicle Tunnels, Sheffield, UK, p.115-150.

Zhao, J., Li, R.X., 2009. Numerical analysis of aerodynamics of high-speed trains running into tunnels. *Journal of Southwest Jiaotong University*, **44**(1):96-100 (in Chinese).

Zhao, W.C., Gao, B., Wang, Y.X., 2006. Numerical investigation of micro pressure wave radiated from the exit of a railway tunnel. *Journal of Basic Science and Engineering*, **14**(3):444-453 (in Chinese).